

Impacts of four northern-hemisphere teleconnection patterns on atmospheric circulations over Eurasia and the Pacific

Tao Gao^{1,2} · Jin-yi Yu² · Houk Paek²

Received: 30 July 2015 / Accepted: 31 March 2016
© Springer-Verlag Wien 2016

Abstract The impacts of four teleconnection patterns on atmospheric circulation components over Eurasia and the Pacific region, from low to high latitudes in the Northern Hemisphere (NH), were investigated comprehensively in this study. The patterns, as identified by the Climate Prediction Center (USA), were the East Atlantic (EA), East Atlantic/Western Russia (EAWR), Polar/Eurasia (POLEUR), and Scandinavian (SCAND) teleconnections. Results indicate that the EA pattern is closely related to the intensity of the subtropical high over different sectors of the NH in all seasons, especially boreal winter. The wave train associated with this pattern serves as an atmospheric bridge that transfers Atlantic influence into the low-latitude region of the Pacific. In addition, the amplitudes of the EAWR, SCAND, and POLEUR patterns were found to have considerable control on the “Vangengeim–Girs” circulation that forms over the Atlantic–Eurasian region in winter or spring. The EA and EAWR mainly affect the westerlies in winter and spring and the POLEUR and SCAND, respectively, in summer and winter. Strong westerlies confine the extension of the North Polar vortex, which generally results in a small weak vortex and a shallow East Asian trough located in a position further east than normal. Furthermore, the North Polar vortex presents significant connections with the patterns during winter and summer. Analyses in this work suggest that the teleconnection patterns

in summer could be driven, at least partly, by the Atlantic Multidecadal Oscillation, which to some degree might transmit the influence of the Atlantic Ocean to Eurasia and the Pacific region.

1 Introduction

As one of the major components of teleconnection patterns, atmospheric extra-long waves influence climatic evolutionary processes. Abnormal oscillations of these extra-long waves generally result in regional or wider-scale irregular atmospheric circulations that can lead to abnormal climatic events elsewhere in the world. Therefore, because of their importance in climate research, considerable attention is given to teleconnection patterns on various timescales. The North Atlantic oscillation, Arctic oscillation, and North Pacific oscillation are examples of dipole circulation patterns with twin oppositely active centers in the zonal direction (Walker and Bliss 1932; Van Loon and Rogers 1978; Rogers 1981; Thompson and Wallace 1998). Other types of teleconnection pattern display wave train characteristics with more than three active centers that are generally aligned in the meridional direction, e.g., the Pacific North America, Eurasia (EU), and eastern Atlantic (EA) upper-air patterns, first identified by Wallace and Gutzler (1981). The EU pattern is focused on sea level pressure (SLP) in winter. This EU pattern is regarded as conventional EU pattern (hereafter referred to as C-EU pattern) in the literature of Liu et al. (2014). In its positive phase, the Siberian High is strong and it expands westward, whereas when the EU pattern exhibits negative polarity, a prevailing zonal circulation extends from the Himalayas to the northern polar region over Eurasia (Smoliak 2009). Based on the analysis methods of digital filtering and spatial correlation, Esbensen (1984) performed a comparative

✉ Tao Gao
frautao@yahoo.com

¹ Inner Mongolia Meteorological Institute, Hailaer Str. 49, Autonomous Region, Hohhot 010051, Inner Mongolia, People's Republic of China

² Department of Earth System Science, University of California, Irvine, Irvine, CA, USA

investigation of interannual and intermonth teleconnections at 700 hPa. Some of the major teleconnection patterns that were clearly defined in the intermonth signals are referred to as the Western Pacific, Western Atlantic, and Pacific–North American patterns in early literature. Other studies have suggested that some teleconnections could be divided into either intermonth or interannual features, which could lead to some different dynamic characteristics (e.g., Esbensen 1984). Panagiotopoulos et al. (2002) summarized the inconsistencies in location and differences of characteristics of teleconnection patterns in the published literature using different datasets, periods, and methods to define teleconnection patterns at the geopotential heights of 700 and 500 hPa and at SLP. The Pacific Decadal Oscillation displays a lagged response to North Atlantic forcing, which is demonstrated by the Atlantic Multidecadal Oscillation (AMO) index. Conversely, climatic change over the North Pacific also affects the AMO (Zhang and Delworth 2007). In addition, a recent study referred to three types of EU pattern in the boreal winter. The method of the rotated empirical orthogonal function was used to extract the teleconnection patterns at the geopotential height of 500 hPa. All three patterns displayed a clear quasi-barotropic wave train structure but with dissimilar sources and active centers, which resulted in different effects on the precipitation and temperature in China. It is considered that the EU pattern is likely driven by abnormal sea surface temperature (SST) in the North Atlantic Ocean (Liu et al. 2014).

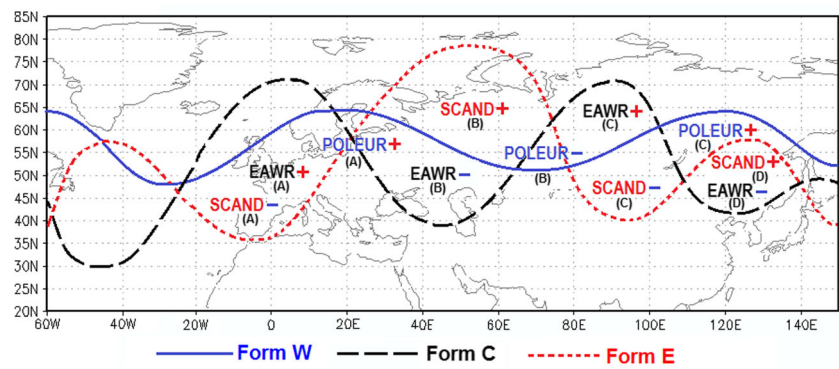
Two Eurasian patterns called EU-1 and EU-2 have been identified at the geopotential height of 700 hPa (Barnston and Livezey 1987). These two teleconnection patterns are also named the Scandinavian (SCAND) and East Atlantic/Western Russia (EAWR) patterns on the website of the Climate Prediction Center (CPC) of the National Oceanic and Atmospheric Administration of the USA (<http://www.cpc.ncep.noaa.gov/data/teledoc/telecontents.shtml>). Hereafter, we use the terms SCAND and EAWR in reference to the EU-1 and EU-2 patterns, respectively. The Polar/Eurasia teleconnection pattern (POLEUR), as defined by the CPC, is a mode that is apparent in all seasons at 700 hPa.

The Eastern Atlantic and Eurasian continent constitute the area upstream of the Asia–Pacific sector. Therefore, the EA, EAWR, POLEUR, and SCAND patterns were the teleconnections selected for this study since their active centers are located in the upstream area. The Eurasia and Pacific sectors are the downstream regions of the upstream area. Concerning of climate forecasting for the downstream regions, the influences of these teleconnections on some of the major atmospheric circulation components need to be investigated in detail. Abnormalities of the teleconnection patterns and those components might provide useful signals for climate prediction in the downstream sectors. The components include the Hadley cell, Walker circulation, westerlies in the mid–high latitudes, subtropical high, East Asian trough, and North Polar vortex.

Some published research has shown that abnormal activities of the western Pacific subtropical high (WPSH), East Asian trough, and North Polar vortex could influence precipitation, temperature, drought, and the frequency of spring dust storms over East Asia. (LinHo et al. 2008; Coy et al. 2009; Wen et al. 2009; Gao and Han 2010; Zhao et al. 2010; Gao et al. 2014). For instance, the interannual variation of the low-frequency oscillation over the mid–high latitudes of Eurasia has been identified as closely connected to the C-EU teleconnection pattern in boreal winter (Yang et al. 2014). Another study has indicated that the winter mid-tropospheric westerly circulation is responsible for the transportation of moisture to the semiarid area of central Asia, which is influenced by both the EAWR and the POLEUR during the winter half of the year (Yin et al. 2014). The zonal oscillation between the WPSH and SST variations on a subseasonal timescale has been linked with persistent heavy rainfall events over the middle and lower reaches of the Yangtze River in China, which occur when the WPSH stretches further westward (Ren et al. 2013). Wang and He (2015) focus on causes of the severe drought occurred in North China and northeastern Asia in 2014 and named two teleconnections as Silk Road and Pacific–Japan pattern. Their analyses indicate that strong intensities of the Silk Road, Pacific–Japan, and C-EU patterns affect the WPSH and East Asian trough that were responsible for the strong precipitation anomaly in North China and large areas of northeastern Asia in the summer of 2014. Additionally, other investigations have examined the circulation changes during a weak cycle of the stratospheric polar vortex and have assessed the associated impact on temperature variation over East Asia. The temperature fluctuation was found crucially influenced by the East Asian trough, which could have been coupled with the stratospheric circulation during the weak polar vortex event (Woo et al. 2015).

Abnormal weather and climatic phenomena result from unusual large-scale atmospheric circulation patterns. The positions of ridges and troughs along the meridional direction control the shape of the long-wave trains that might bring different weather and climate to specific regions (Sidorenkov and Orlov 2008; Hoy et al. 2013, 2014). Russian scientists Vangengeim (Вангенгейм) and Girs (Гирс) sorted various types of atmospheric circulation over the Atlantic and Eurasia continent into three forms that are known collectively as the “Vangengeim–Girs” classification. The three types of circulation are generally referred to as form W (solid line), C (dashed line), and E (dotted line) in Fig. 1. Form W occurs when the basic westerlies move zonally in the Northern Hemisphere (NH) with a series of small short-wave troughs and ridges. Form C occurs when quasi-stationary long-wave trains with large amplitude exist, with two ridges established over the eastern part of the Atlantic Ocean and central parts of Asia, and two troughs located over western areas of the continent and the east coast of Asia. Comparing form E with form C

Fig. 1 Locations of the active centers of the EAWR and SCAND for wintertime, the POLEUR for spring season, and the Atlantic-Eurasian long wave troughs and ridges of the Vangengeim–Girs classification forms W (solid line), C (dashed line), and E (dotted line)



reveals opposite trough–ridge positions of the wave trains in form E. Thus, in this form, central and eastern Europe is usually controlled by a strong ridge at high levels that could lead to a strong upward flow around the Aral Sea and the Caspian Sea and force the Siberian High to move eastward (Vangengeim 1935, 1940; Bolotinskaja and Ryzhakov 1964; Girs 1971, 1974; Girs and Kondratovich 1978).

Many published studies referring to teleconnection patterns have focused on the mid–high latitudes (Watanabe and Nitte 1999; Wen et al. 2009; Liu and Chen 2012). However, some research has considered the impact of teleconnections on the Tibetan Plateau (Li et al. 2008), extreme drought in the Iberian Peninsula during 2004–2005 (Garcia-Herrera et al. 2007), and the Bay of Biscay (Cozannet et al. 2011). In this study, we

Table 1 The major atmospheric circulation indices for Eurasia and Pacific regions

Circulation system	Index	Brief explanation
Subtropical high West Pacific: 110° E–180°; East Pacific: 175°–115° W; Pacific: 110° E–115° W	Area	Total grids with geopotential height ≥ 588 gpdm in the range 10°–60° N of a specific longitude sector in $5^\circ \times 10^\circ$ horizontal resolution of the monthly mean geopotential height at 500 hPa.
	Intensity	Average of numbered grids with geopotential height ≥ 588 gpdm in the range 10°–60° N of a specific longitude sector in $5^\circ \times 10^\circ$ horizontal resolution of the monthly mean geopotential height at 500 hPa. (588 gpdm numbered 1; 589 gpdm numbered 2; 590 gpdm numbered 3, etc.).
	North boundary	Averaged latitudes at the cross points between north branch 588 gpdm line and the longitudes within specific meridional sector in $5^\circ \times 10^\circ$ horizontal resolution of the monthly mean geopotential height at 500 hPa.
	West extension point	Longitude of the most west point of 588 gpdm between meridional sector 90° E–180° of the West Pacific subtropical high in $5^\circ \times 10^\circ$ horizontal resolution of the monthly mean geopotential height at 500 hPa.
North Polar vortex Asia: 60°–150° E; North Hemisphere: 5° E–360°	Area	Northern area confined by featured isoheight which mostly approaches the maximum westerly axes between specific range of two longitudes in 500 hPa monthly mean weather chart
	Intensity	Air mass between two geopotential heights of 500 hPa mean isoheight and the featured isobaric surface mentioned above.
Eastern Asia trough	Position	Averaged position (longitude) of the trough line in rectangle of 110°–170° E and 30°–50° N at 500 hPa geopotential height
	Intensity	Difference between the maximum and minimum geopotential heights in rectangle of 110°–170° E and 30°–50° N at 500 hPa monthly mean geopotential height.
Zonal index over Eurasia		Averaged air mass zonal transported through unit cubes/per unit time over Eurasia (0°–150° E).
Meridional index over Eurasia		Averaged air mass meridional transported through unit cubes/per unit time over Eurasia (0°–150° E).
Vangengeim–Girs circulation form W		Differences of the position and intensity between ridges and troughs over the Atlantic and Europe. The zonal circulation is prevailing with a flat westerly belt in 500 hPa monthly mean weather chart.
Vangengeim–Girs circulation form C		Differences of the position and intensity between ridges and troughs over the Atlantic and Europe. The west coast of Europe is controlled by a ridge, a long wave covers the Ural area, and meridional circulation is prevailing in 500-hPa monthly mean weather chart.
Vangengeim–Girs circulation form E		Differences of the position and intensity between ridges and troughs over the Atlantic and Europe. The Ural area is controlled by a ridge and the meridional circulation is prevailing over East Asia in 500 hPa monthly mean weather chart.

considered not just the atmospheric circulation components in the mid–high latitudes but also over the tropical region of the Asia–Pacific sector. Furthermore, we also explored the connections between the AMO and the selected teleconnection patterns, and the correlations between the teleconnection patterns, the Vangengeim–Girs circulation forms, the westerlies, and the major atmospheric circulation components including the WPSH, East Asian trough, and North Polar vortex.

The remainder of this paper is organized as follows. Section 2 describes the data and method used in the study. Section 3 examines the atmospheric circulation impacts of the teleconnection patterns. Possible impacts of the AMO on the teleconnection patterns are investigated in Sect. 4. A summary and some discussions are presented in Sect. 5.

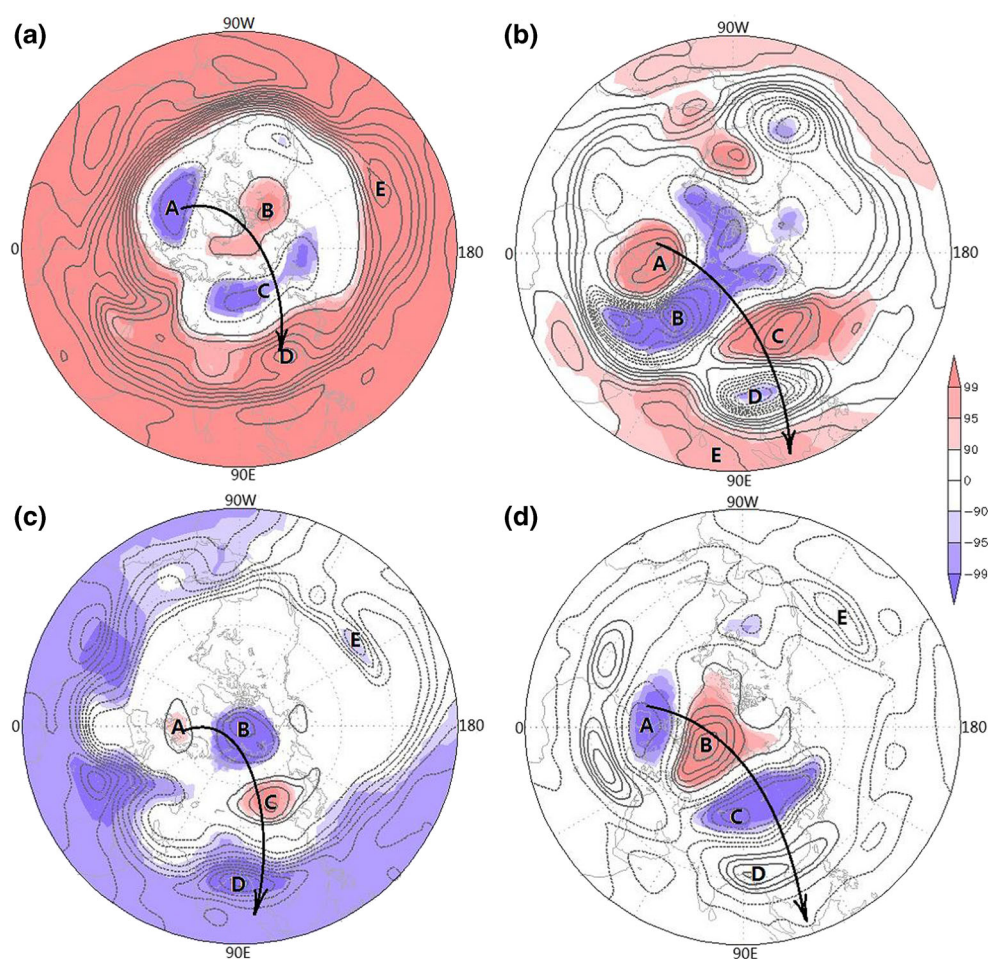
2 Data and methodology

In this study, we used monthly geopotential SLP and zonal and meridional winds (denoted U- and V-winds, respectively) from the reanalysis dataset of the National Center of Environmental Prediction/National Center for

Atmospheric Research (NCEP/NCAR) (Kalnay et al. 1996; downloaded from <http://www.esrl.noaa.gov/psd>). The analyses focused specifically on the period of 1950–2013 (64 years). Monthly anomalies were obtained by removing the mean seasonal cycles based on the period from 1981 to 2010. We also used the seasonal means of boreal spring (March–May), summer (June–August), fall (September–November), and winter (December–February), unless otherwise specified.

Several indices were used in this study. The indices for the EA, EAWR, POLEUR, and SCAND teleconnection patterns were defined as the 3rd, 6th, 8th, and 9th principal components of a rotated principal component analysis of the monthly 500-hPa height anomalies in the NH (poleward of 20° N). The monthly EA, EAWR, POLEUR, and SCAND indices were downloaded from the website of the CPC (<http://www.cpc.ncep.noaa.gov/data>). The major atmospheric circulation component indices (Table 1), including the subtropical high, North Polar vortex, East Asian trough, zonal and meridional circulations, and Atlantic–Europe patterns were provided by the National Climate Center of the China Meteorological Administration (<http://ncc.cma.gov.cn/Website/index.php?ChannelID=5>).

Fig. 2 Pattern regressions on the geopotential heights at 500 hPa for winter (a EA, b EAWR, c POLEUR, d SCAND) with statistical confidence levels (A, B, C, D, and E stand for pressure centers)



The monthly intensity index (I_{Δ}) of the westerly belt over Eurasia (0° – 150° E) was determined using the following formula:

$$I_{\Delta} = I_Z / I_{Zmean} - I_M / I_{Mmean} \quad (1)$$

where I_Z and I_M denote the monthly zonal and meridional circulation index, respectively. The I_Z represents the averaged zonal air mass transport through a unit cube per unit time over Eurasia (0° – 150° E), and I_M denotes the averaged meridional air mass movement through a unit cube per unit time over Eurasia. The specific equations for the calculation of I_Z and I_M can be found in Zhao (1999). The parameters I_{Zmean} and I_{Mmean} are the 30-year climatological means from 1981 to 2010. The seasonal I_{Δ} was obtained by averaging the index of the 3 months in winter and summer. A zonal circulation prevails when the value of I_{Δ} is above zero and a meridional circulation is predominant when I_{Δ} is below zero.

The Equator zonal wind index representing the Walker circulation is calculated as the vertical shear of the zonal wind between 850 and 200 hPa over the tropical Pacific (5° S– 5° N, 180° – 100° W). The Hadley circulation index is computed as the vertical shear of the meridional wind between 200 and

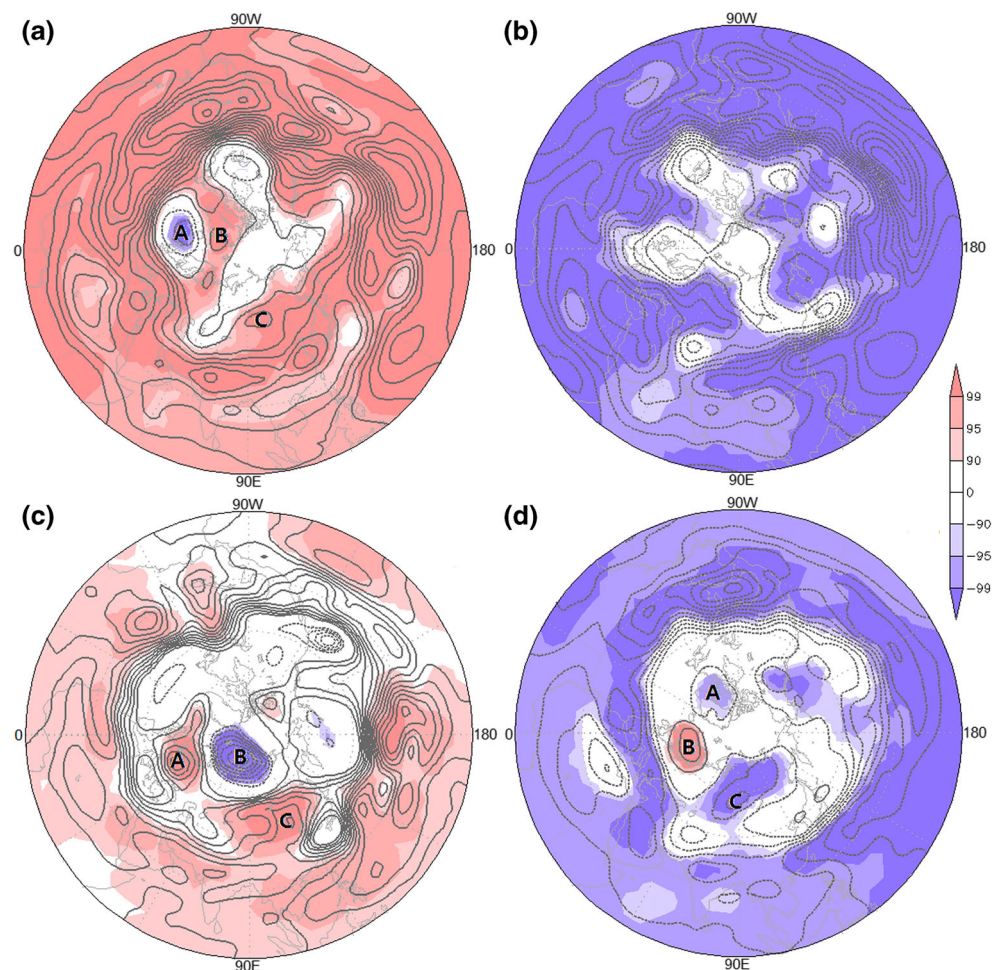
850 hPa for the sectors of India (65° – 95° E, 0° – 30° N), the West Pacific (110° E– 180° , 0° – 30° N), and the Pacific (110° E– 115° W, 0° – 30° N) (Oort and Yinger 1996). The AMO index is defined as the area-averaged SST anomalies over the North Atlantic (Enfield et al. 2001), and this information was downloaded from <http://www.esrl.noaa.gov/psd>.

We performed composite, regression, and correlation analyses as part of this study. For the composite analysis, we objectively divided the 64-year samples into three groups: above normal (21 samples), normal (22 samples), and below normal (21 samples) for each index. We refer to the above and below normal groups as HIGH and LOW groups, respectively. To determine the statistical significance, we used Student's t test and a bootstrapping procedure (BSP) with 1000 times resampling (von Storch and Zwiers 1999).

3 Impacts on atmospheric circulations over Eurasia and the Pacific

Spatial structures, statistically significant areas, and positive and negative active centers of the EA, EAWR, POLEUR, and

Fig. 3 As in Fig. 1 but for summer season (a EA, b EAWR, c POLAUR, d SCAND)



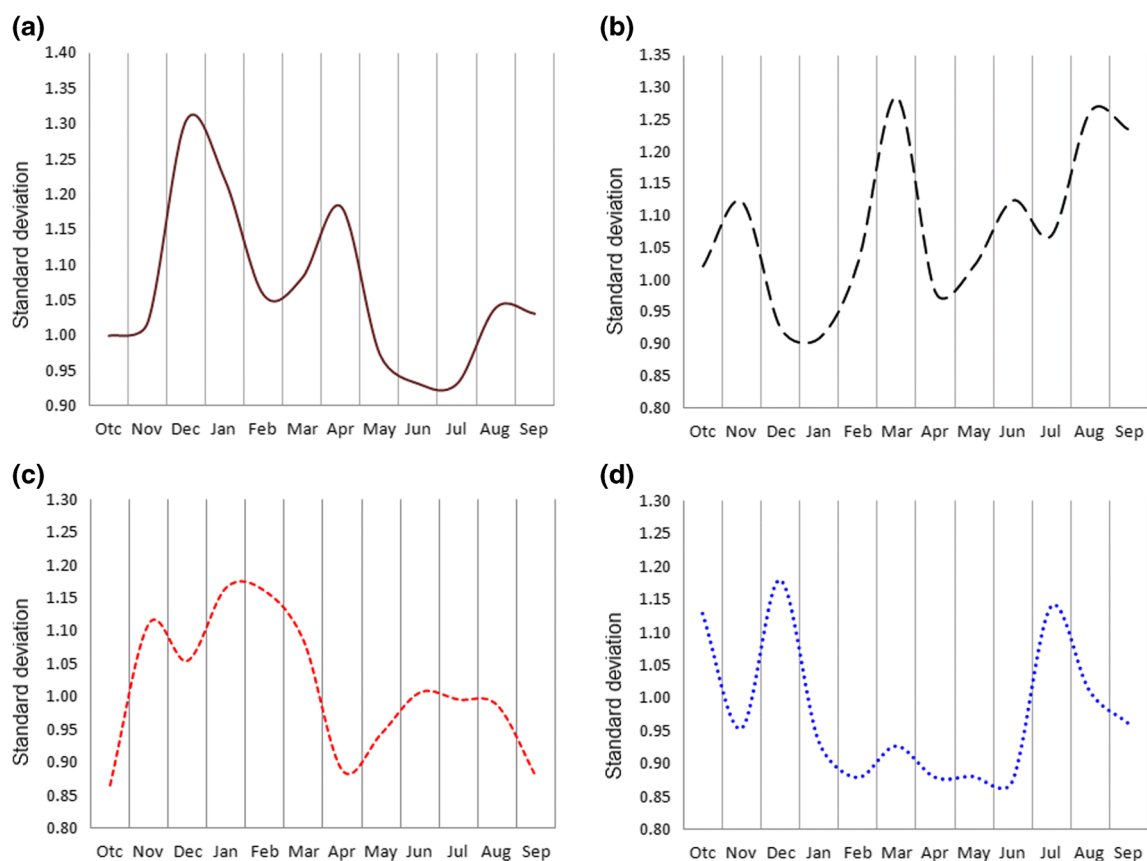


Fig. 4 Monthly standard deviations of the four teleconnection patterns (**a** EA, **b** EAWR, **c** POLEUR, **d** SCAND)

SCAND patterns for winter and summer can be viewed by regressing the 500-hPa geopotential height anomalies onto their indices (Figs. 2 and 3). Their monthly standard deviations present their characteristics of seasonality. The EA pattern is more active during winter and spring (Fig. 4a), and the EAWR pattern is most active from spring to fall (Fig. 4b). The active season of the POLEUR pattern is from November to the following March (Fig. 4c), and the SCAND pattern shows an active period from fall to winter (Fig. 4d).

3.1 Impacts on north polar vortex

As mentioned earlier, the North Polar vortex is a major influential atmospheric circulation component in the NH (Zhang et al. 2006, 2008, 2014; Wang and Ding 2009). We calculated the correlation coefficients between the indices of the four teleconnections and the North Polar vortex for the Asia (60° – 150° E) and Pacific (150° E– 120° W) sectors. As shown in Table 2, we found that the summer EA and EAWR patterns

Table 2 Correlation coefficients between the EA, EAWR, POLEUR, and SCAND patterns and the North Polar vortex indices

North Polar vortex		EA		EAWR		POLEUR		SCAND	
		Summer	Winter	Summer	Winter	Summer	Winter	Summer	Winter
Asia (60° – 150° E)	Area intensity	–0.520 ^a	–0.360 ^a	0.498 ^a	–0.167	–0.274 ^b	–0.020	0.315 ^b	0.449 ^a
		–0.410 ^a	0.229	0.500 ^a	0.187	0.412 ^a	0.356 ^a	0.586 ^a	0.265 ^b
Pacific (150° E– 120° W)	Area intensity	–0.674 ^a	0.105	0.466 ^a	–0.227	–0.053	–0.018	0.287 ^b	0.096
		–0.537 ^a	0.245 ^c	0.660 ^a	0.316 ^b	0.006	–0.050	0.300 ^b	–0.028

^a>99 % statistical confidence level

^b95 % statistical confidence level

^c90 % statistical confidence level

are significantly (>99 % level) correlated with the North Polar vortex for both sectors, whereas they are less correlated during winter. The significant negative correlation with the EA pattern in summer implies that the North Polar vortex shrinks in the Asian–Pacific sector and that this is accompanied by the positive geopotential height at low–high latitudes. This feature is shown explicitly in the regressed height anomaly pattern in Fig. 3a. The findings from the correlation and regression analyses are verified by the composite analysis. The values of the North Polar vortex indices composited for the HIGH and LOW groups of the teleconnection indices are shown in Table 3. It can be seen that the HIGH (LOW) group of the EA index tends to accompany small (large) values of the vortex indices, which is consistent with the negative correlations (Table 2). Similarly, the 500-hPa geopotential height composited for the HIGH EA index group (Fig. 5a) shows a smaller North Polar vortex than that of the LOW index group (Fig. 5b). In contrast to the summer EA pattern, the EAWR pattern shows positive correlations with the North Polar vortex (Table 2), indicating an extension of the North Polar vortex accompanied by negative height regressions at low–high latitudes (Fig. 3b). The composite analyses also show that the HIGH (LOW) EAWR index group tends to accompany large (small) values of the vortex indices (Table 3) and a larger (smaller) vortex area in the Asian–Pacific sector (Fig. 5c, d). The POLEUR pattern does not show any obvious correlations with the North Polar vortex. The summer SCAND pattern displays positive correlations with the North Polar vortex (Table 2), consistent with an expanded North Polar vortex with negative height regressions at low–high latitudes (Fig. 3d). The HIGH (LOW) SCAND index group accompanies large (small) values of the vortex indices (Table 3) and a smaller (larger) vortex area in the Asia–Pacific sector (Fig. 5e, f).

As an important component of the NH, the effects of the North Polar vortex on the climate of China and on the

Table 3 Summer mean values of the North Polar vortex indices composited for HIGH and LOW groups of the four teleconnection patterns

Pattern		Asia (60°–150° E)		Pacific (150° E–120° W)	
		Area	Intensity	Area	Intensity
EA	L	157.4	28.2	177.8	36.5
	H	142.3	25.7	161.5	31.6
EAWR	L	144.0	26.0	166.3	32.0
	H	157.2	28.9	176.1	37.4
POLEUR	L	152.2	25.6	–	–
	H	144.8	28.6	–	–
SCAND	L	146.2	25.6	168.1	33.5
	H	153.4	29.4	173.8	36.2

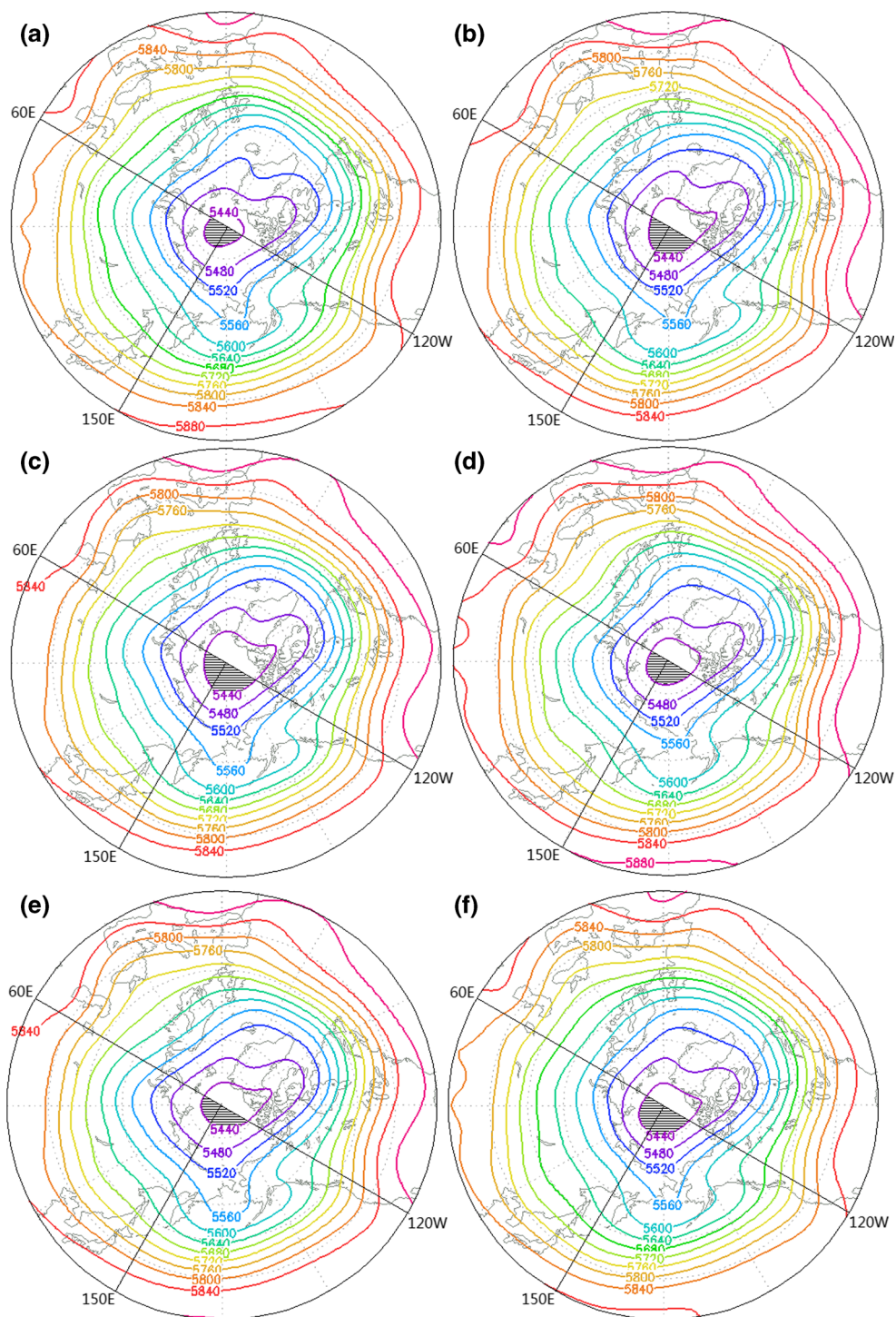
L and H denote the LOW and HIGH groups, respectively

atmospheric circulations over Eurasia have been considered in previous work (Zhang et al. 2008, 2014; Wang and Ding 2009). Although the four selected patterns have been found significantly associated with the North Polar vortex in summer and winter, some close correlations have also been found to exist between the patterns of the leading seasons and the vortex of the following season. For instance, the spring POLEUR pattern has significant connection to the summer vortex in terms of both its area and its intensity indices. The coefficients between them were 0.41 and 0.37 (>99 % level) for area and intensity, respectively. In addition, the summer EA pattern has close correlations with the area and intensity of the autumn vortex, evidenced by the statistical correlation coefficients of -0.46 for the area and -0.42 for the intensity (>99 % level). However, the patterns have been identified as being closely associated with the westerly belt over the Eurasian continent. A zonal circulation may prevail when the westerly belt is strong, which corresponds to a smaller and intense vortex. It is suggested that the teleconnection patterns in the previous terms might provide some seasonal forecast signals for the North Polar vortex and for climate prediction in specific regions.

3.2 Impacts on mid–high-latitude circulations

To examine the influences of the teleconnection patterns on the atmospheric circulation from over the Eurasia continent, we superimposed the active centers of the teleconnection patterns (Figs. 2 and 3) onto the forms W, C, and E of the stationary wave trains in Fig. 1. The two positive height anomaly centers (or anticyclones) of the EAWR pattern over Western Europe and Siberia in winter coincide with the two ridges of the form C wave trains (dashed line). The two negative centers (or cyclones) around Eastern Europe and East Asia coincide with the two troughs of form C. This in-phase relationship between the EAWR pattern and form C of the atmospheric circulation is also confirmed by the correlation coefficient of 0.63 (>99 % level) between the EAWR and form C indices. The two anticyclones in the far west of Siberia and northern East Asia of the SCAND pattern in winter correspond to the two ridges of form E (dotted line), and the two cyclones over southwestern parts of Europe and central Asia correspond to the two troughs of this form. The correlation coefficient between the indices of the SCAND pattern and form E was 0.53 (>99 % level). In spring, the POLEUR pattern has two positive and one negative height anomaly centers that are coincident with the two ridges and one trough of form W (solid line). The correlation coefficient between them was -0.61 (>99 % level). These analyses suggest that strong EAWR and SCAND patterns can accompany large-amplitude ridges and troughs over the continent that lead to effective meridional exchanges of warm and cold air and humidity. In contrast, a strong POLEUR pattern can accompany small-amplitude ridges

Fig. 5 Mean geopotential heights at 500 hPa for HIGH and LOW groups of EA (a HIGH, b LOW), EAWR (c HIGH, d LOW), and SCAND (e HIGH, f LOW) for summer season (the lined area is below 5440 mb)



and troughs that lead to a belt of strong westerlies at mid–high latitudes that inhibits exchange between the north and south.

Different circulation forms determine dissimilar patterns of weather and climate in different regions (Sidorenkov and Orlov 2008; Zhao 1999; Hoy et al. 2013, 2014). The wave trains of the EAWR and SCAND patterns display contrasting shapes (Fig. 1). This raises the question of whether a trigger exists that leads to exchange between the wave trains of the

EAWR pattern (fitted to form C) and those of the SCAND pattern (fitted to form E). If such a trigger could be identified, the further question would be how long such exchange processes could be maintained. This interesting question should be very meaningful for climatologists wishing to predict long-term climate for specific regions.

The influences of the teleconnection patterns on the forms of atmospheric circulation over Eurasia can be identified

further when considering the correlations with the westerly belt in the mid–high latitudes that extends from the western coast to eastern areas of the Eurasian continent. A zonal circulation that prevails when the westerly belt is strong might block the exchanges of thermal energy and humidity between the north and south. Conversely, greater trough and ridge activities might occur when a meridional circulation pattern dominates the continent, associated with a weak westerly belt. It has been proven in this study that all four of the teleconnection patterns have varying degrees of impact on the intensity and shape of the westerly belt. This fact is definitely demonstrated by the significant coefficients of correlation between the pattern indices and the westerly index (I_{Δ}) presented in Table 4.

A zonal circulation prevails when the value of I_{Δ} is positive. In this case, the southward extension of the North Polar vortex usually retreats poleward, blocked by the relatively flat westerly belt. This fact is identified by the significant correlations between I_{Δ} and the indices of the North Polar vortex exhibited in Table 5. A negative value of I_{Δ} is associated with a strong meridional circulation. Under this condition, cyclones and anticyclones are more likely to become established over the continent, meaning that the North Polar vortex could extend further south, bringing colder air to regions of lower latitude.

The EA and EAWR patterns have been evidenced mainly affecting the intensity of the westerly belt in winter and spring. The POLEUR and SCAND patterns exert their obvious influences during spring–summer and winter, respectively (Table 4). The intensity and shape of the westerly belt are controlled by the intensities and positions of the active centers of these four teleconnection patterns. Comparing the mean anomaly UV-wind fields of the HIGH group for the teleconnection pattern indices with those of the LOW group clearly reveals contrasting features of the westerly belt (Fig. 6). A cyclone can be seen over Siberia for the HIGH group of the EA pattern during winter (Fig. 6a), which corresponds to one of the negative centers of the EA. It indicates that the southern boundary of this strong and elliptical cyclone might produce a westerly belt that is stronger than normal. The opposite situation appears in the anomaly wind field for the LOW group of the EA pattern,

Table 4 Correlation coefficients between the indices of the teleconnection patterns and the westerly (I_{Δ}) over Eurasia (0° – 150° E)

Pattern	Spring	Summer	Winter	Winter–Spring
EA	0.508 ^a	0.142	0.594 ^a	0.586 ^a
EAWR	0.457 ^a	0.115	0.380 ^a	0.503 ^a
POLEUR	0.267 ^b	0.394 ^a	0.081	0.077
SCAND	0.063	−0.158	−0.447 ^a	−0.286 ^a

^a>99 % statistical confidence level

^b95 % statistical confidence level

Table 5 Correlation coefficients between the westerly (I_{Δ}) and atmospheric circulation indices for Eurasia and Pacific

Element	Index Name	Winter	Winter–Spring
Polar vortex of Asian range (60° – 150° E)	Area	−0.589 ^a	−0.477 ^a
	Intensity	0.308 ^b	0.348 ^a
Eastern Asia trough	Position	0.348 ^a	–
	Intensity	0.259 ^b	–

^a>99 % statistical confidence level

^b95 % statistical confidence level

i.e., the cyclone in Fig. 6a is replaced by an anticyclone and the wind direction correspondingly changes into winds from the northeast (Fig. 6b). This highlights how a weak EA vibration might result in a weak westerly belt over Eurasia. There are contrasting wave shapes of the westerly belt with large amplitudes shown in the mean wind fields of the HIGH and LOW groups for the EAWR and SCAND patterns, which indicate a prevailing meridional circulation over the Eurasian continent. When the EAWR pattern is in a positive phase, a cyclone is present between two anticyclones over the continent for the HIGH group of the EAWR, and the westerly belt is stronger than normal (Fig. 6c). In the opposite case, the westerly belt is weaker than normal, as evidenced by the reversed wind directions (Fig. 6d). There is a large and strong anticyclone embedded between two cyclones from the north direction around 20° – 60° E for the HIGH group of the SCAND pattern. It results in a weak westerly belt that is expressed by the eastern wind anomalies (Fig. 6e). In contrast, a strong westerly belt is established in association with a weak SCAND pattern (Fig. 6f). For the HIGH group of the POLEUR pattern, two anticyclones around the mid–high-latitude range coexist with a large cyclone covering the North Polar area. The combined functions of the cyclone and anticyclones result in a strong westerly belt (Fig. 6g). The situation is reversed for the LOW group of the pattern in connection with a weak POLEUR pattern during summer (Fig. 6h).

The East Asian trough that generally appears over the eastern coast of Asia is one of the major stationary waves in winter in the NH. Different positions and intensities of the trough might result in dissimilar weather and climate in different regions upstream of the trough, e.g., areas of China and Mongolia (Yang and Zhang 1994; Wang et al. 2012; Huang et al. 2013). Cold air masses from Siberia normally move southeastward with the flux through the trough, triggering cold waves over the region. Close correlations exist between the I_{Δ} and the trough indices that represent the indirect influences of the EA, EAWR, and SCAND patterns in winter (Table 4). The trough is evidently connected to the westerly belt because of the significant coefficient of correlation between them (Table 5). It might be weaker and remain in a

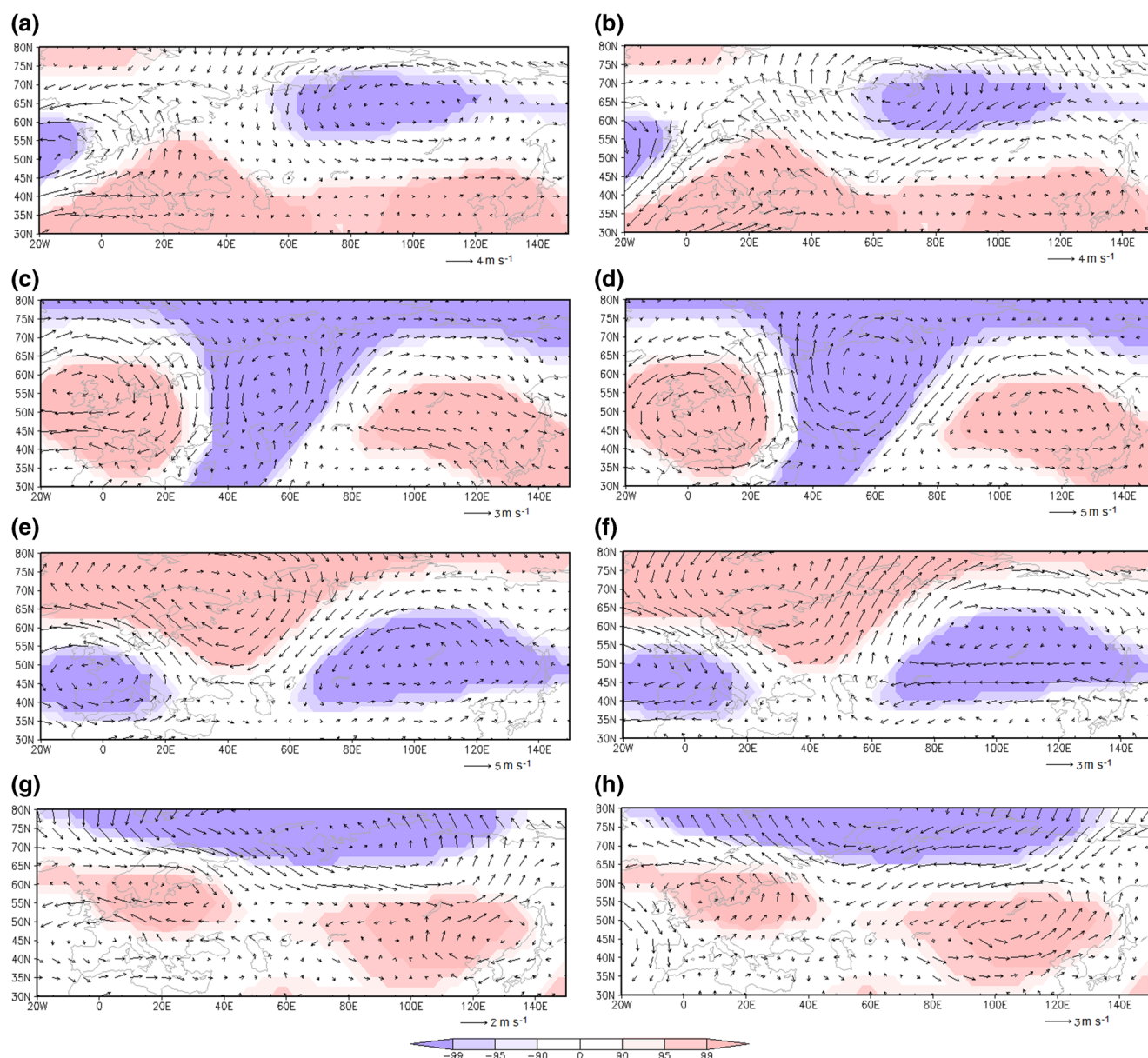


Fig. 6 Mean anomaly UV-wind at 500 hPa for high and low groups of the westerly plus above 90 % significant regression areas in both left and right side for EA (**a** HIGH, **b** LOW), EAWR (**c** HIGH, **d** LOW), SCAND

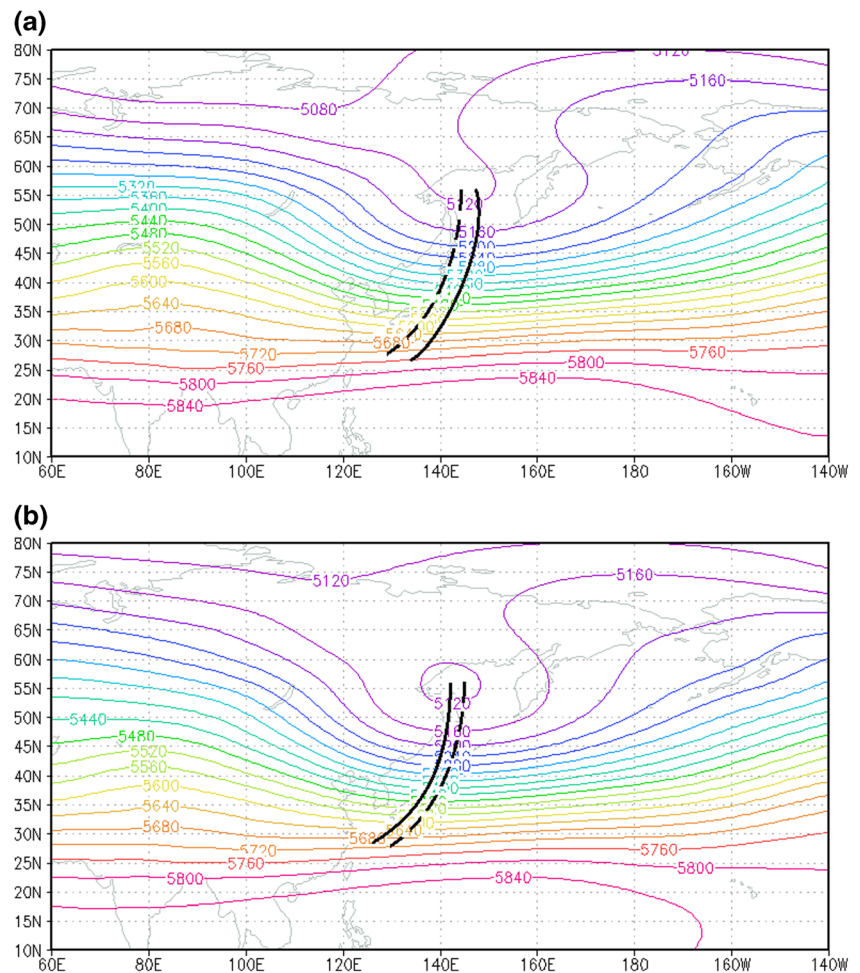
(**e** HIGH, **f** LOW) for wintertime, and POLEUR for summer season (**g** HIGH, **h** LOW)

position further east in association with a prevailing zonal circulation indicated by higher intensity indices of the westerly belt (Fig. 7a). Conversely, it would be stronger and remain in a location further west when the westerly belt is weak (Fig. 7b). Furthermore, another active center marked “D” is located around the position of the East Asia trough (Fig. 2b). The EAWR pattern is correlated closely to the position and intensity of the trough in winter, as evidenced by the coefficients of correlation of 0.48 and 0.30 (>99 % and >95 % level) for the position and intensity, respectively. A zonal circulation prevails with a strong westerly belt when the EAWR pattern is in a positive phase. A large anticyclone occupies most of northern Asia for the HIGH group of the EAWR pattern

(Fig. 6c), which pushes the trough further eastward. The trough is shallow because of the prevailing zonal circulation. Conversely, a cyclone can be seen located in the southeast in the LOW group of the pattern (Fig. 6d). The trough becomes deeper and moves to western position when the pattern is in a negative phase with a meridional circulation condition.

The analyses above should be meaningful for climatologists because they may extract some forecast signals from the phases of the teleconnection patterns that match the Vangengeim–Girs classification forms and affect the principal atmospheric circulation components, such as the westerly belt and the East Asia trough in the mid-high latitudes.

Fig. 7 Mean geopotential heights at 500 hPa for the HIGH (a) and LOW groups (b) of the westerly for wintertime (the *solid curves* denote the trough lines and the *dashed line* is climatology position of the trough line; contour interval 40 gpm)



3.3 Impacts on subtropical circulations

Published research refers to linkages between the Atlantic–Europe and Asia–Pacific regions that are largely attributable to the influences of the EU, North Atlantic oscillation, and Arctic oscillation teleconnection patterns. Most studies have

focused on the mid–high latitudes (Li et al. 2008; Sung et al. 2009; Qian and Liang 2012; Takaya and Nakamura 2013; Liu et al. 2014). Here, we explored the possible impacts of our selected teleconnection patterns on the circulation components in the lower latitudes. The subtropical highs over different sectors of the NH, e.g., the WPSH, have significant influence on

Table 6 Correlation coefficients between the EA pattern and subtropical high indices

Subtropical high		EA pattern				
		Annual	Spring	Summer	Autumn	Winter
North Hemisphere	Area	0.609 ^a	0.462 ^a	0.496 ^a	0.343 ^b	0.517 ^a
	Intensity	0.656 ^a	0.474 ^a	0.500 ^a	0.480 ^a	0.457 ^a
Pacific (110° E–115° W)	Area	0.567 ^a	0.405 ^a	0.379 ^b	0.278 ^c	0.566 ^a
	Intensity	0.496 ^a	0.335 ^a	0.360 ^b	0.227	0.540 ^a
West Pacific (110° E–180°)	Area	0.600 ^a	0.456 ^a	0.311 ^b	0.322 ^b	0.569 ^a
	Intensity	0.413 ^a	0.362 ^a	0.252 ^c	0.242 ^c	0.544 ^a
	North boundary	0.269 ^c	0.305 ^b	0.081	−0.155	0.513 ^a
	West extension point	−0.500 ^a	−0.340 ^a	−0.144	−0.308 ^b	−0.590 ^a

^a >99 %, statistical confidence level

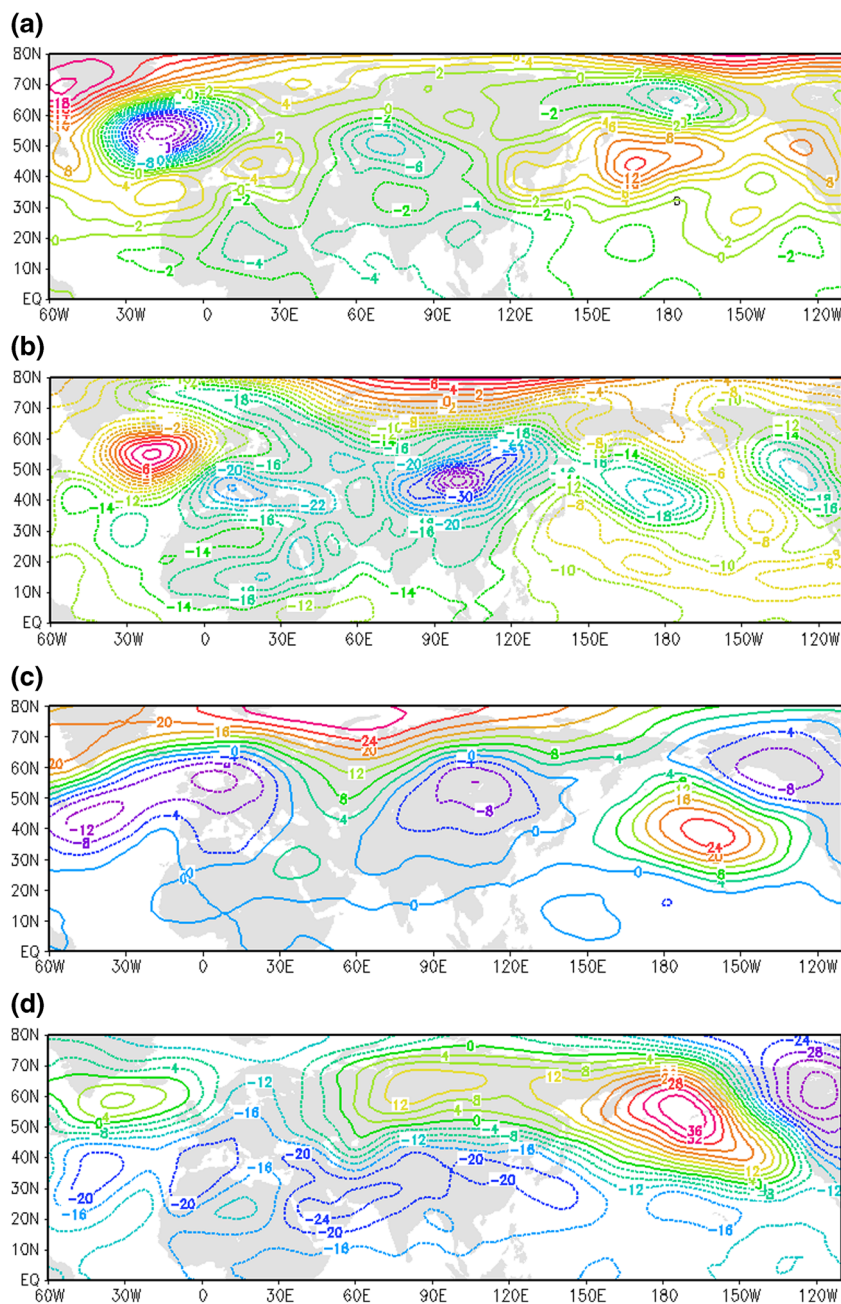
^b 95 % statistical confidence level

^c 90 % statistical confidence level

the weather and climate of China (Luo et al. 2005; Duan et al. 2008; Huang et al. 2012; Zhao et al. 2012). To examine the relationships between the teleconnections and the subtropical high, we used subtropical high indices involving intensity, area, and the northern boundary. It has been found that the EA pattern is closely correlated with the subtropical high, confined not only within the West Pacific sector but also in the subtropical region of the NH throughout all seasons (Table 6). The significant positive correlations imply that positive geopotential anomalies occur in the EA pattern in both winter and summer (Figs. 2a and 3a). Composited geopotential height anomalies

also demonstrate that the HIGH group of the EA pattern is accompanied by a strong and northward-extending subtropical high (Fig. 8a, c), whereas the LOW group tends to correspond to a weak subtropical high (Fig. 8b, d). Furthermore, the summer EAWR and SCAND patterns with negative anomalies at low–high latitudes hint at close relationships with the subtropical high (Fig. 3b, d). Significant (>99 % level) correlation coefficients of -0.48 and -0.35 were found between the subtropical high index and the EAWR and SCAND indices, respectively, whereas there was no significant correlation found between the POLEUR pattern and the subtropical high.

Fig. 8 Mean geopotential height anomaly at 500 hPa for HIGH and LOW groups of EA pattern in summer (**a** HIGH, **b** LOW; contour interval 2 gpdm) and winter (**c** HIGH, **d** LOW; contour interval 4 gpdm)



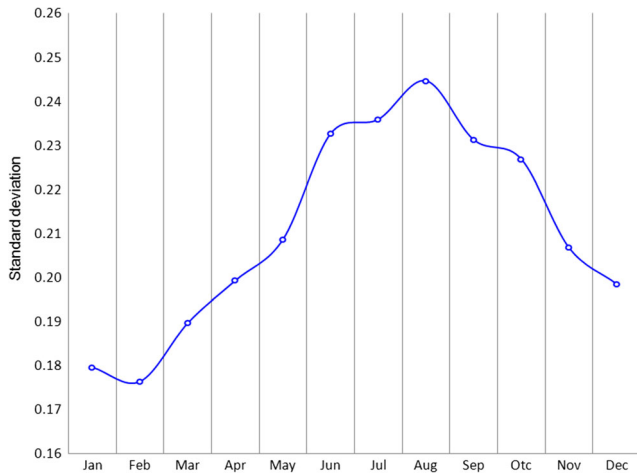


Fig. 9 Monthly standard deviations of the AMO

4 Connections between the AMO and teleconnection patterns

This section examines the relationships between the four selected teleconnection patterns and decadal variations in the Atlantic SST. The latter is represented by the AMO index. It can be found from the monthly standard deviations of the

AMO index that the most active period of SST variation is from June to September, i.e., the warm months in the NH (Fig. 9). By regressing the SLP and 500-hPa geopotential height onto the AMO index (Fig. 10), negative SLP regressions appear in the western half of the NH and positive values appear in the eastern half near the surface (Fig. 10a, b). During the positive AMO phase, positive SST anomalies over the North Atlantic basin can directly warm the air mass above, leading to low SLP anomalies centered over the basin and extending downstream toward the European and African continents (in the western half of the NH). In response to the poleward oceanic heat transport in the North Atlantic and Pacific, the mid-latitude jet stream over the North Pacific moves poleward. This results in a redistribution of the air mass and causes high SLP anomalies in the North Pacific that are centered off the west coast of North America and extend toward the central to western Pacific (in the eastern half of the NH) (e.g., Zhang and Delworth 2007). Furthermore, significant anomalies are found not only over the Atlantic Ocean but also in the low–mid-latitude regions of the Pacific Ocean, especially during summer. In the mid-troposphere (Fig. 10c, d), the AMO is related positively with the geopotential height anomalies in most of the NH. Over the warm North Atlantic basin,

Fig. 10 Regressions of AMO onto SLP and 500 hPa geopotential height for winter (a, c) and summer seasons (b, d) with statistical confidence levels

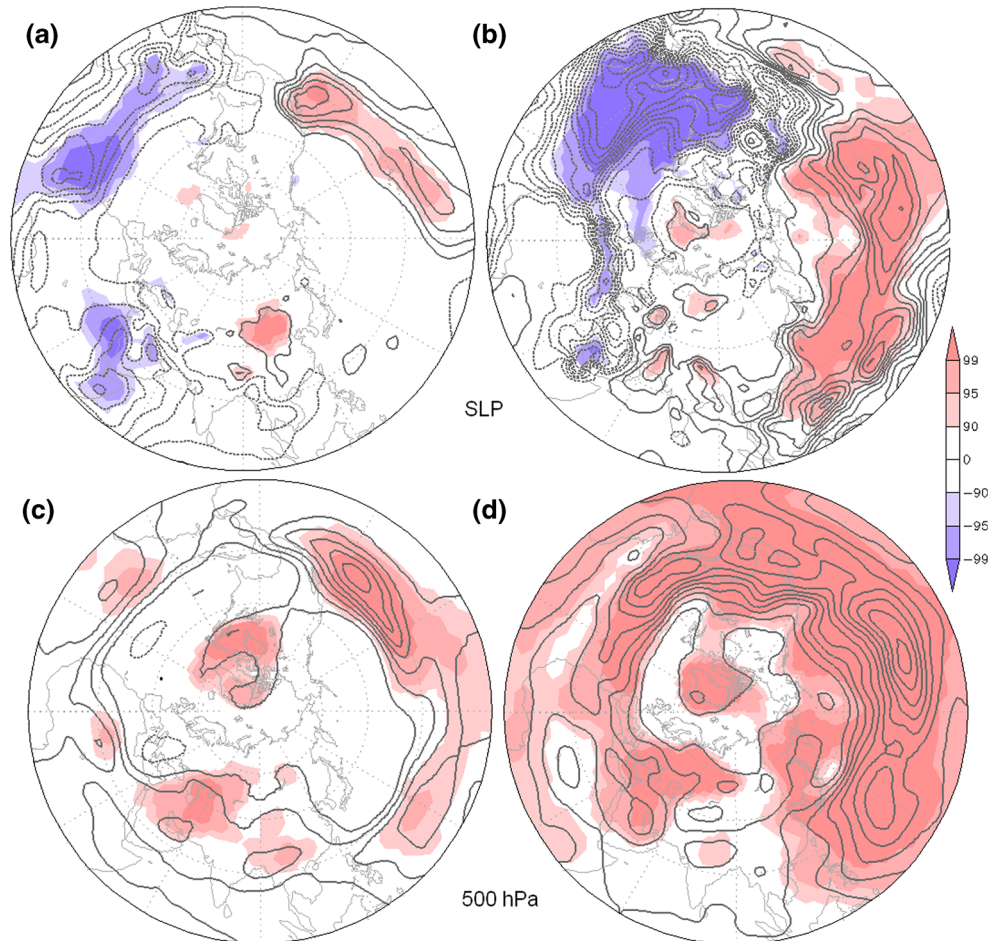


Table 7 Correlation coefficients between the AMO and EA, EAWR, POLEUR, and SCAND indices

EA			EAWR			POLEUR			SCAND		
ANN	SUM	WIN	ANN	SUM	WIN	ANN	SPR	WIN	ANN	SUM	WIN
0.377 ^b	0.467 ^a	-0.004	-0.443 ^a	-0.588 ^a	-0.122	-0.323 ^b	-0.374 ^a	0.038	-0.282 ^b	-0.310 ^b	-0.061

^a>99 % statistical confidence level^b95 % statistical confidence level

tropospheric temperatures throughout the entire depth of the troposphere can increase. Then, this tropospheric warming, particularly in the region of the tropics to the extratropics, spreads zonally throughout the entire low-latitude region (e.g., Kumar and Hoerling 2003; Lau et al. 2005). This results in positive geopotential height anomalies along a low-latitude belt (centered around 20° N). The AMO-associated Central Pacific El Niño can also support troposphere warming and positive height anomalies in the mid-troposphere (Yu et al. 2015). This is why the regressed SLP anomaly pattern shows a dipole structure between the western and eastern halves of the NH, while the 500-hPa height anomaly pattern exhibits an in-phase structure over most of the NH, centered along the low latitudes.

The correlation coefficients were calculated between the indices of the four selected teleconnection patterns and the AMO, as shown in Table 7. The AMO is significantly correlated with the EA, EAWR, and SCAND patterns in summer and with the POLEUR pattern in spring. These close relationships are further confirmed by the correlations between the AMO-regressed patterns and the teleconnections for SLP and geopotential height anomalies at 300 and 500 hPa (Table 8). To examine the impact of the AMO on the patterns, we performed a BSP and the results are shown in Table 9. The results indicate that the AMO significantly (>99 % level) affects the EA, EAWR, and SCAND patterns during summer, whereas it does not significantly influence the POLEUR pattern during spring. Our analyses only assessed the effects of the AMO on the four selected patterns for contemporaneous seasons. Some studies have referred to the influence of the AMO on some oscillations; e.g., the Eurasian–Pacific multidecadal oscillation has displayed concurrent fluctuations with the AMO since the beginning of the 20th century (Lee and Hsu 2013), and ENSO forcing can strongly modify

Table 8 Pattern correlations between regression fields of the AMO and EA, EAWR, POLEUR, and SCAND patterns

AMO	EA(SUM)	EAWR(SUM)	POLEUR(SPR)	SCAND(SUM)
300 hPa	0.888 ^a	-0.929 ^a	-0.653 ^a	-0.837 ^a
500 hPa	0.851 ^a	-0.909 ^a	-0.730 ^a	-0.821 ^a
SLP	0.420 ^a	-0.676 ^a	-0.530 ^a	-0.200 ^b

^a>99 % statistical confidence level^b90 % statistical confidence level

the atmospheric circulation variations driven by the AMO (Hu and Feng 2012). However, the mechanisms linking the AMO with the teleconnection patterns, lagged correlations, principal influential factors, and possible forecast signals require further exploration.

The BSP in this study identified the influence of the AMO on the EA, EAWR, and SCAND patterns but not on the POLEUR pattern. The 70.9 % statistical confidence level for spring POLEUR pattern does not satisfy the normally required confidence level (Table 9). However, a confidence level of 96.8 % was achieved when the POLEUR pattern was set as the independent variable and the AMO considered as the dependent variable in the BSP. This suggests that the POLEUR pattern might conduct atmospheric forcing on the AMO. Further evidence was presented by the significant correlation coefficients between the spring POLEUR pattern and the AMO of the following seasons that reached -0.50 and -0.48 (>99 % level) for the summer and autumn and -0.38 (>95 % level) for winter. The influence of the POLEUR pattern on the AMO is an interesting subject that remains to be investigated. It was not explored in this study because the focus was on the effects of the AMO upon the selected teleconnection patterns.

5 Summary and discussion

5.1 Summary

A comprehensive investigation of the influences of the EA, EAWR, POLEUR, and SCAND teleconnection patterns on various areas of the NH, from the North Polar Region to the

Table 9 The bootstrapping procedure results for impacts of the AMO on the EA, EAWR, POLEUR, and SCAND patterns

Element	5-Low	5-High	Difference(H-L)	Confidence (%)
AMO→EA (summer)	-0.988	0.533	1.521	99.9
AMO→EAWR (summer)	0.668	-0.713	1.381	99.5
AMO→POLEUR (spring)	0.194	0.011	0.183	70.9
AMO→SCAND (summer)	0.976	-0.479	1.455	99.9

tropics, and of their associations with the AMO was performed in this study. For the North Polar region, some significant correlations exist between the selected teleconnection patterns and the polar vortex, mainly in summer and winter. The EA pattern is correlated negatively with the vortex in the Asia–Pacific sector during summer, whereas the EAWR and SCAND patterns are correlated positively. The POLEUR pattern has positive influence on the intensity of the vortex over Asia in both winter and summer. The SCAND pattern has a positive effect on both the area and the intensity of the vortex in the Asia sector in winter. Furthermore, the mean geopotential heights at 500 hPa for the HIGH and LOW groups of the patterns provided further evidence of these close connections.

Different atmospheric circulation forms that lead to different locations of the ridges and troughs in the mid–high latitudes result in dissimilar climatic regimes for different regions. It was found that the stationary wave trains of the EAWR and SCAND patterns fit perfectly into the long-wave patterns of the form C and E Vangengeim–Girs classification over the Eurasian continent in winter, whereas the POLEUR pattern controls the form W circulation type during spring. Furthermore, all of the four patterns presented close connections with the

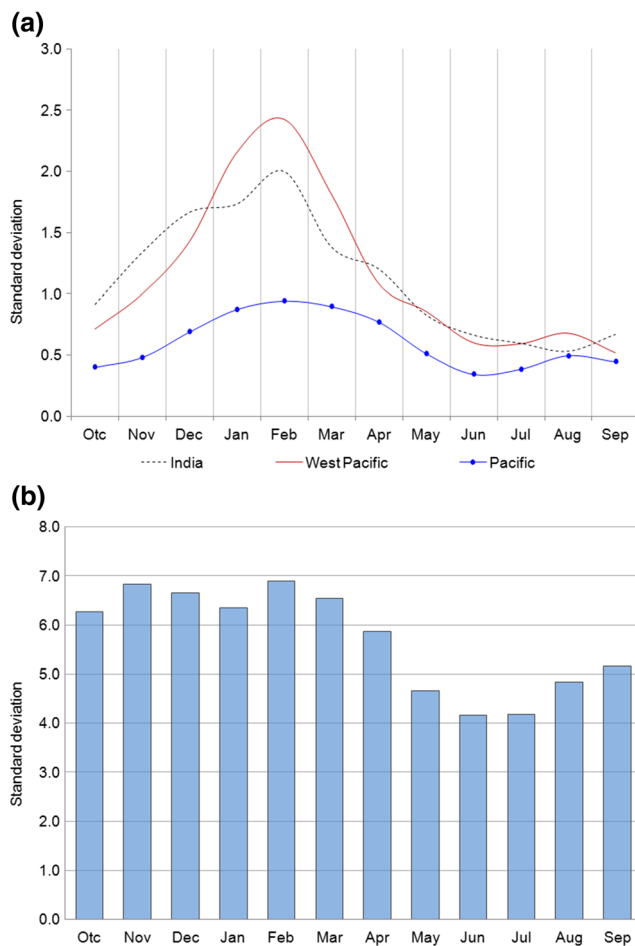


Fig. 11 Monthly standard deviation of Hadley and Walker intensity index (**a** Hadley, **b** Walker)

Table 10 Correlation coefficients between the Hadley, Walker cells, and EA and EAWR teleconnection pattern indices for winter

HI (India) (65°–95°E)		HI (Pacific) (110°E–115° W)		EZWI (Walker) (180°–100° W)	
EA	EAWR	EA	EAWR	EA	EAWR
0.377 ^a	0.530 ^a	–0.436 ^a	–0.370 ^a	0.311 ^b	0.311 ^a

^a>99 % statistical confidence level

^b95 % statistical confidence level

intensity of the westerly belt over Eurasia in winter, spring, and summer. A strong westerly belt presents a prevailing zonal circulation that restricts the southward extension of the North Polar vortex over the Asia–Pacific sector. This situation generally corresponds to positive phases of the EA, EAWR, and POLEUR patterns and the negative phase of the SCAND pattern, which result in a shrunken but strong vortex and a shallow East Asian trough with a position that is further east than normal.

The wave train of the EA pattern not only influences the mid–high-latitude regions but it also affects the overall tropical and subtropical belt of the NH in all seasons. Winter is the season affected most significantly by the EA pattern. The subtropical highs in different sectors of the NH are large and strong with northward extension when the EA pattern is in its positive phase and vice versa. Additionally, the EAWR and SCAND patterns negatively influence the subtropical high in the entire NH, primarily in summer.

As a crucial element of the Atlantic Ocean, the AMO represents the variation of the SST of the Atlantic. Outcomes of the statistical time series, pattern correlation analyses, and the BSP evidenced the actual effects of the AMO on the EA, EAWR, and SCAND patterns, principally in summer. The AMO positively affects the EA pattern, and it is negatively connected with the EAWR and SCAND patterns. These three patterns have roles as atmospheric bridges that transfer influential signals from the Atlantic Ocean to the Eurasia and Pacific regions. The analyses and outcomes of this study should be meaningful for climatologists wishing to derive forecast signals from Atlantic Ocean SST and the phases of teleconnection patterns.

Table 11 The bootstrapping procedure results for the EA and EAWR influences on the Walker and Hadley cells in winter season

Element	5-L	5-H	Difference(H-L)	Confidence (%)
EA → Hadley (Pacific)	1.015	–1.343	2.358	99.0
EAWR → Hadley (India)	0.494	–0.902	1.396	99.0
EA → Walker	2.751	–1.753	4.504	97.3
EAWR → Walker	–3.796	4.819	8.615	99.0

L and H denote the LOW and HIGH groups, respectively

5.2 Discussion

Most published research relating to teleconnection patterns has focused on analyzing and distinguishing the temporal characteristics and spatial structures at mid–high latitudes, primarily in winter (Wallace and Gutzler 1981; Esbensen 1984; Barnston and Livezey 1987; Panagiotopoulos et al. 2002; Liu et al. 2014). In this study, we investigated the correlations between certain teleconnection patterns and some atmospheric circulation components from the North Polar Region to the tropics of Eurasia and the Pacific in all seasons. Although some connections were found, many topics concerning the influences of the teleconnection patterns in the Asia and Pacific regions remain to be explored.

The Hadley and Walker cells are two major controlling components of the NH atmospheric circulation, the intensities of which vary consistently during all months of the year. The cold period in the NH is their active season, as presented by the monthly standard deviations in comparison with the warm period (Fig. 11a, b). The correlation coefficients between the winter–spring Walker cell (180°–260° E) and the western Pacific (110° E–180°) and Pacific (110° E–115° W) Hadley cells were -0.81 and -0.73 , respectively (0.01 significance level). It has been identified in this study that the EA and EAWR teleconnection patterns have close associations with the intensities of the Hadley and Walker cells. The EAWR pattern mainly presents a significant positive correlation with the Indian Hadley cell (65°–95° E), and the EA pattern has a negative connection with the Pacific Hadley cell during winter. Outputs of the BSP analysis further identified significant influences of the EA and EAWR patterns on the Pacific and Indian Hadley cells at statistical confidence levels of 99.0 %. The intensity of the Walker circulation is positively connected to the EA and EAWR patterns in winter (Table 10). Furthermore, the BSP suggested that the impacts of the EA and EAWR patterns on the Walker intensity reached the 97.3 and 99.0 % statistical confidence levels, respectively (Table 11). The dynamic mechanisms via which the EA and EAWR patterns affect the Walker and Hadley cells is an interesting topic that should be investigated in the future.

In this study, we analyzed only the contemporaneous correlations between the teleconnection patterns and some major atmospheric circulation systems. To explore the effects of the patterns for previous seasons and to determine stable forecasting signals would be of greater interest to climate forecasters, because leading signals obtained from prior periods would enable forecasters to perform timely predictions.

Acknowledgments The first author would like to thank the China Scholarship Council (CSC) and the University of California, Irvine, USA, for the financial support and provision of a pleasant working environment during her period as a senior visiting scholar. Cordial thanks are extended to the anonymous reviewers and editors for their constructive comments and suggestions for the improvement of this paper. Many thanks are offered to

Professor Jinyi Yu for his suggestions concerning the presented topic. The authors appreciate the help given by Dr. Fangting Yu regarding the improvement of the written English. This study was supported by the US National Science Foundation (AGS-1233542 and AGS-1505145), National Natural Science Foundation of China (No. 40965007), Natural Science Foundation of Inner Mongolia, China (No. 2013MS0923), and Financial Support for Scientific Research of Inner Mongolia Meteorological Bureau, China Meteorological Administration (No. nmqxljcx201607).

References

- Barnston AG, Livezey RE (1987) Classification, seasonal and persistence of low-frequency atmospheric circulation patterns. *Mon Wea Rev* 115:1083–1126
- Bolotinskaja MS, Ryzhakov LJ (1964) Katalog makrosinoptičeskikh protsessov po klassifikacij G.J. Vangengeima 1891–1962 [catalogue of macro-synoptic processes according to the G.J. Vangengeim's classification 1891–1962; in Russian]. AANII Leningrad, p. 158
- Coy L, Eckermann S, Hopple K (2009) A planetary wave breaking and tropospheric forcing as seen in the stratospheric sudden warming in 2006. *J Atmos Sci* 66:495–507
- Cozannet GL, Lecacheux S, Delvallee E, Desramaut N, Oliveros C, Pedreros R (2011) Teleconnection pattern influence on sea-wave climate in the Bay of Biscay. *J Clim* 24:641–652
- Duan LY, Huang YS, Liang PD (2008) Effect of West Pacific subtropical high on summer precipitation in North China. *Meteorol Sci Technol* 36(3):273–276
- Enfield DB, Mestas-Nunez AM, Trimble PJ (2001) The Atlantic multidecadal oscillation and its relationship to rainfall and river flows in the continental U.S. *Geophys Res Lett* 28:2077–2080
- Esbensen SK (1984) A comparison of intermonthly and interannual teleconnections in the 700 mb geopotential height field during the northern hemisphere winter. *Mon Wea Rev* 112:2016–2032
- Gao T, Han JW (2010) Evolutionary characteristics of the atmospheric circulations for frequent and infrequent dust storm springs in Northern China and the detection of potential future seasonal forecast signals. *Meteorol Appl* 17:76–86
- Gao T, Han JW, Gao L, Yan W (2014) Impacts of North India Ocean SST on the extremely cold winters of 2011 and 2012 in the region of Da Hinggan Mountains and its western areas in China. *Theor Appl Climatol* 117:693–705
- Garcia-Herrera R, Paredes D, Trigo RM, Trigo IF, Hernandez E, Barriopedro D, Mendes MA (2007) The outstanding 2004/05 drought in the Iberian Peninsula: Associated atmospheric circulation. *J Hydrometeorol* 8:483–498. doi:10.1175/JHM578.1
- Girs AA (1971) Mnogoletnije kolebanija atmosfernoj cirkuljacii idolgosročnyje gidrometeorologičeskije prognozy. [Many-year fluctuations of atmospheric circulation and long-term hydrometeorological forecasts; in Russian]. *Gidrometeotzdat*, Leningrad, p. 280 pp
- Girs AA (1974) Makrocirkuljacionnyj metod dolgosročnyh meteorologičeskikh prognozov [macro-circulation method of long-term meteorological forecasts; in Russian]. *Gidrometeotzdat*, Leningrad, 488 pp
- Girs AA, Kondratovich LI (1978) Metody dolgosročnyh prognozov pogody [methods of long-term weather forecast; in Russian]. *Gidrometeotzdat*, Leningrad, p. 343 pp
- Hoy A, Sepp M, Matschullat J (2013) Large-scale atmospheric circulation forms and their impact on air temperature in Europe and Northern Asia. *Theor Appl Climatol* 113:643–658. doi:10.1007/s00704-012-0770-3
- Hoy A, Schucknecht A, Sepp M, Matschullat J (2014) Large-scale synoptic types and their impact on European precipitation. *Theor Appl Climatol* 116:19–35. doi:10.1007/s00704-013-0897-x
- Hu Q, Feng S (2012) AMO- and ENSO-driven summertime circulation and precipitation variations in North America. *J Clim* 25:6477–6495

- Huang L, He JH, Lu CY (2012) Review and outlook of researches about Western Pacific subtropical high (in Chinese with an English abstract). *J Arid Meteorol* 30(2):225–260
- Huang XM, Guan ZY, Dai ZJ, Mei HX (2013) A further look at the interannual variations of east Asian trough intensity and their impacts on winter climate of China (in Chinese with an English abstract). *Acta Meteorologica Sinica* 71(3):416–428
- Kalnay E et al. (1996) The NCEP/NCAR 40-year reanalysis project. *Bull Amer Meteor Soc* 77:437–471
- Kumar A, Hoerling MP (2003) The nature and causes for the delayed atmospheric response to el Niño. *J Clim* 16:1391–1403
- Lau NC, Leetmaa A, Nath MJ, Wang HL (2005) Influences of ENSO-induced indo–Western Pacific SST anomalies on extratropical atmospheric variability during the boreal summer. *J Clim* 18:2922–2942
- Lee MY, Hsu HH (2013) Identification of the Eurasian–North Pacific multidecadal oscillation and its relationship to the AMO. *J Clim* 26:8139–8153
- Li J, Yu RC, Zhou TJ (2008) Teleconnection between NAO and climate downstream of the Tibetan plateau. *J Clim* 21:4680–4690
- LinHo LH, Huang XL, Lau NC (2008) Winter-to-spring transition in East Asia: a planetary-scale perspective of the South China spring rain onset. *J Clim* 21:3081–3096
- Liu YY, Chen W (2012) Variability of the Eurasian teleconnection pattern in the northern hemisphere winter and its influences on the climate in China (in Chinese with an English abstract). *Chin J of Atmospheric Science* 36(2):423–432
- Liu YY, Wang L, Zhou W (2014) Three Eurasian teleconnection patterns: spatial structures, temporal variability, and associated winter climate anomalies. *Clim Dyn* 42:2817–2839
- Luo L, He JH, Tan YK (2005) The composite features and possible mechanisms during the westward extension of subtropical high in the Western Pacific (in Chinese with an English abstract). *Sci Meteorol Sinica* 25(5):465–473
- Oort AH, Yienger JJ (1996) Observed interannual variability in the Hadley circulation and its connections to ENSO. *J Clim* 9:2751–2767
- Panagiotopoulos F, Shahgedanova M, Stephenson DB (2002) A review of northern hemisphere winter-time teleconnection patterns. *J de Physique* 12(10):27–47. doi:10.1051/jp4:20020450
- Qian WH, Liang HY (2012) Atmospheric teleconnections and regional-scale atmospheric anomalies over the northern hemisphere (in Chinese with an English abstract). *Chinese J Geophys* 55(5):1449–1461
- Ren XJ, Yang XQ, Sun XG (2013) Zonal oscillation of Western Pacific subtropical high and subseasonal SST variations during Yangtze persistent heavy rainfall events. *J Clim* 26:8929–8946
- Rogers JC (1981) The North Pacific oscillation. *Int J Climatol* 1(1):39–57
- Sidorenkov NS, Orlov IA (2008) Atmospheric circulation epochs and climate changes. *Russ Meteorol Hydrol* 33(9):553–559
- Smoliak BV (2009) A Eurasian pattern of northern hemisphere winter-time sea level pressure variability. University of Washington Graduate School, Degree of Master of Science
- Sung MK, Lim GH, Kwon WT, Boo KO, Kug JS (2009) Short-term variation of Eurasian pattern and its relation to winter weather over East Asia. *Int J Climatol* 29:771–775
- Takaya K, Nakamura H (2013) Interannual variability of east Asian winter monsoon and related modulations of the planetary waves. *J Clim* 26:9445–9461
- Thompson DWJ, Wallace JM (1998) The Arctic oscillation signature in the winter geopotential height and temperature fields. *Geophys Res Lett* 25(9):1297–1300
- Van Loon H, Rogers JC (1978) The seesaw in winter temperature between Greenland and Northern Europe. Part I: general description. *Mon Wea Rev* 106:296–310
- Vangengeim GJ (1935) Opyt primenenija sinopticeskih metodov kizuceniju i karakteristike klimata [experimental usage of synoptical methods for studying and characterizing of climate; in Russian]. *Gidrometeotzdat, Moskva*, p. 109 pp
- Vangengeim GJ (1940) Dolgostocnyi prognoz temperatury vozduha Ivskrytija rek [long term forecast of air temperature and river openings; in Russian]. *Trudy GGI* 10
- von Storch H, Zwiers FW (1999) *Statistical analysis in climate research*. Cambridge University Press, Cambridge, pp. pp 93–pp 44
- Walker GT, Bliss EW (1932) *World weather V. Mem. Roy Meteor Soc* 4: 53–84
- Wallace JM, Gutzler DS (1981) Teleconnections in the geopotential height field during the northern hemisphere winter. *Mon Wea Rev* 109:784–812
- Wang ZY, Ding YH (2009) Impacts of the long-term change of the summer Asian polar vortex on the circulation system and the water vapor transport in East Asia (in Chinese with an English abstract). *Chinese J Geophys* 52(1):20–29
- Wang HJ, He SP (2015) The North China/Northeastern Asia severe summer drought in 2014. *J Clim* 28:6667–6681
- Wang WL, Wang JY, Xie YQ, Wang WG, Wang ZW, Wang K, Du LM, Deng NS, Cai SM, Li YL (2012) Analysis of decadal variation of East Asia trough and West Pacific subtropical high in summer (in Chinese with an English abstract). *Adv Earth Sci* 27(3):304–320
- Watanabe M, Nitte T (1999) Decadal changes in the atmospheric circulation and associated surface climate variations in the northern hemisphere winter. *J Clim* 12:494–510
- Wen M, Yang S, Kumar A, Zhang PQ (2009) An analysis of the large-scale climate anomalies associated with the snowstorms affecting China in January 2008. *Mon Wea Rev* 137:1111–1131
- Woo SH, Kim BM, Kug JS (2015) Temperature variation over East Asia during the lifecycle of weak stratospheric polar vortex. *J Clim* 28: 5857–5872
- Yang GY, Zhang Y (1994) The relationship between anomalous trough over East Asia and el Niño (in Chinese with an English abstract). *Q J Applied Meteorol* 5(1):114–118
- Yang SY, Wu BY, Zhang RH, Zhou SW (2014) Propagation of low-frequency oscillation over Eurasian mid-high latitude in winter and its association with Eurasian teleconnection pattern (in Chinese with an English abstract). *Chin J Atmos Sci* 38(1):121–132
- Yin ZY, Wang HL, Liu XD (2014) A comparative study on precipitation climatology and interannual variability in the lower midlatitude East Asia and Central Asia. *J Clim* 27:7830–7848
- Yu JY, Kao PK, Paek H, Hsu HH, Hung CW, Lu MM, An SI (2015) Linking emergence of the Central-Pacific el Niño to the Atlantic multi-decadal oscillation. *J Clim* 28:651–662
- Zhang R, Delworth TL (2007) Impact of the Atlantic multidecadal oscillation on North Pacific climate variability. *Geophys Res Lett* 34(1–6):L23708. doi:10.1029/2007GL031601
- Zhang HD, Lu WS, Gao ST, Zhang YS (2006) Influence of the north polar vortex activity on the contemporaneous and subsequent air temperature in China (in Chinese with an English abstract). *J Nanjing Inst Meteorol* 29(4):507–526
- Zhang HD, Jin RH, Zhang YZ (2008) Relationships between summer northern polar vortex with subtropical high and their influence on precipitation in North China (in Chinese with an English abstract). *J Tropical Meteorol* 24(4):417–422
- Zhang JW, Li DL, Liu YJ (2014) New features of polar vortex and its impacts on winter temperature of China (in Chinese with an English abstract). *Plateau Meteorol* 33(3):721–732
- Zhao ZG (1999) Atmospheric circulation conditions of China flood and drought during summer (in Chinese). *China Meteorological Press, Beijing*, pp. 79–94
- Zhao P, Yang S, Yu RC (2010) Long-term changes in rainfall over Eastern China and large-scale atmospheric circulation associated with recent global warming. *J Clim* 23:1544–1562
- Zhao JH, Feng GL, Yang J, Zhi R, Wang QG (2012) Analysis of the distribution of the large-scale drought/flood of summer in China under different types of the Western Pacific subtropical high (in Chinese with an English abstract). *Acta Meteorol Sinica* 70(5):1011–1031